Supporting Information

Heterostructures Stacked with X_2SY (X=In, Ga; Y=Se, Te) and g-C_2N Monolayers for High Power Conversion Efficiency Solar Cells: Insight from Electronic Properties and Nonadiabatic Dynamics

Xue-Qing Wan [a], Chuan-Lu Yang [a,b,*], Xiaohu Li[b,c], Yuliang Liu [a], and Wenkai Zhao[a]

[a] *School of Physics and Optoelectronic Engineering, Ludong University, Yantai 264025, China*

[b] *Xinjiang Astronomical Observatory, Chinese Academy of Sciences, Urumqi 830011, China*

[c] *Key Laboratory of Radio Astronomy, Chinese Academy of Sciences, Urumqi 830011, China*

1. The geometrical configurations and electronic properties of the monolayers and heterostructures

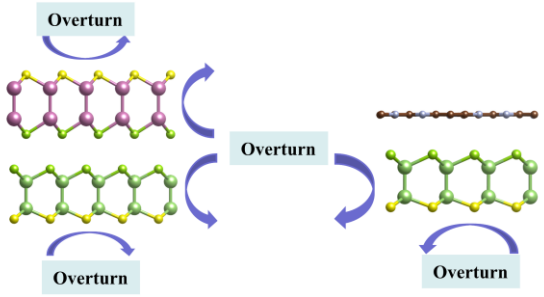

Fig. S1. The different stacking patterns of X_2SY-X_2SY(X=Ga, In; Y=Se, Te) and g-C_2N-X_2SY(X=Ga, In; Y=Se, Te) heterostructures.

*Corresponding author. *E-mail address:* ycl@ldu.edu.cn. (C.L. Yang).

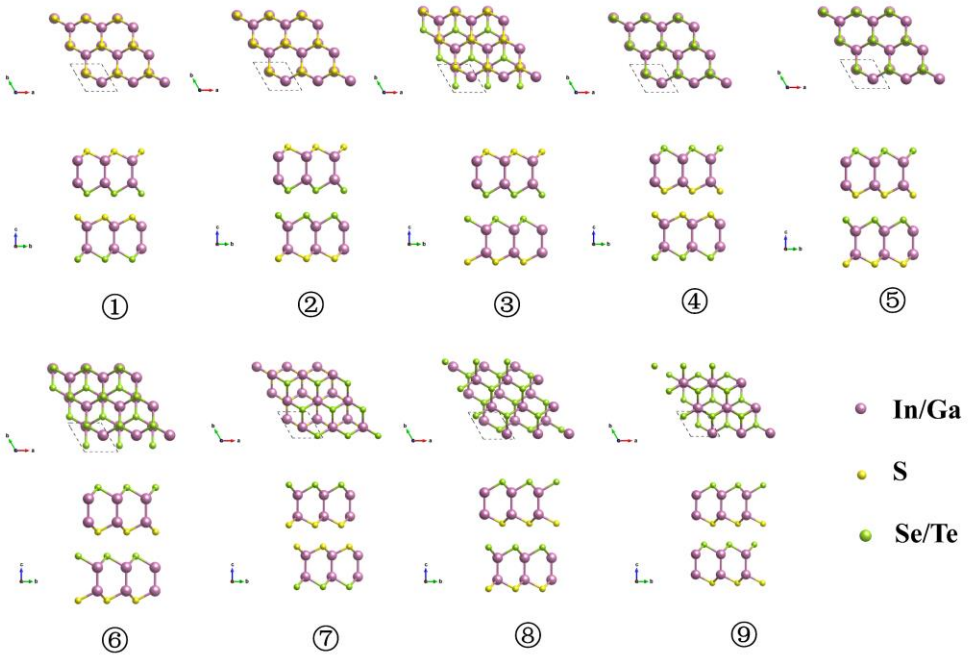

Fig. S2. The 9 different stacking patterns of X_2SY-X_2SY heterostructures.

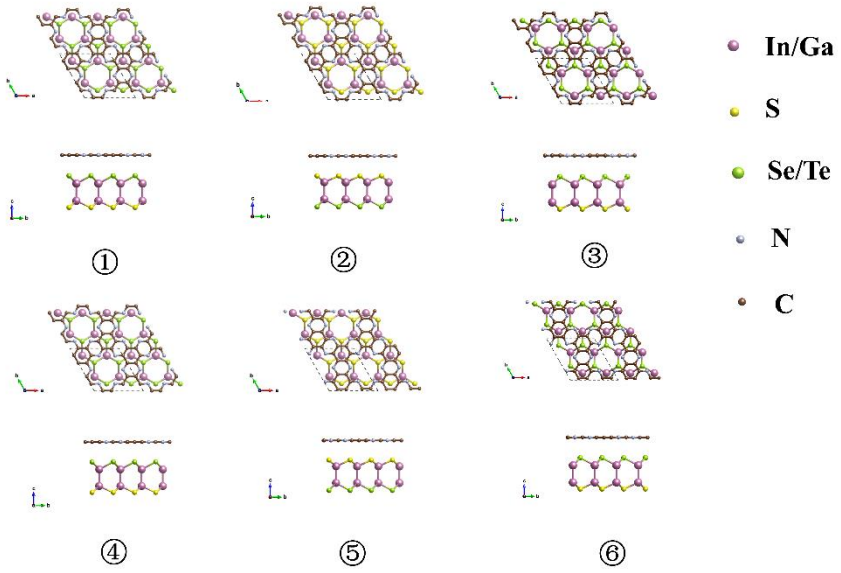

Fig. S3. The 6 different stacking patterns of g-C_2N-X_2SY heterostructures.

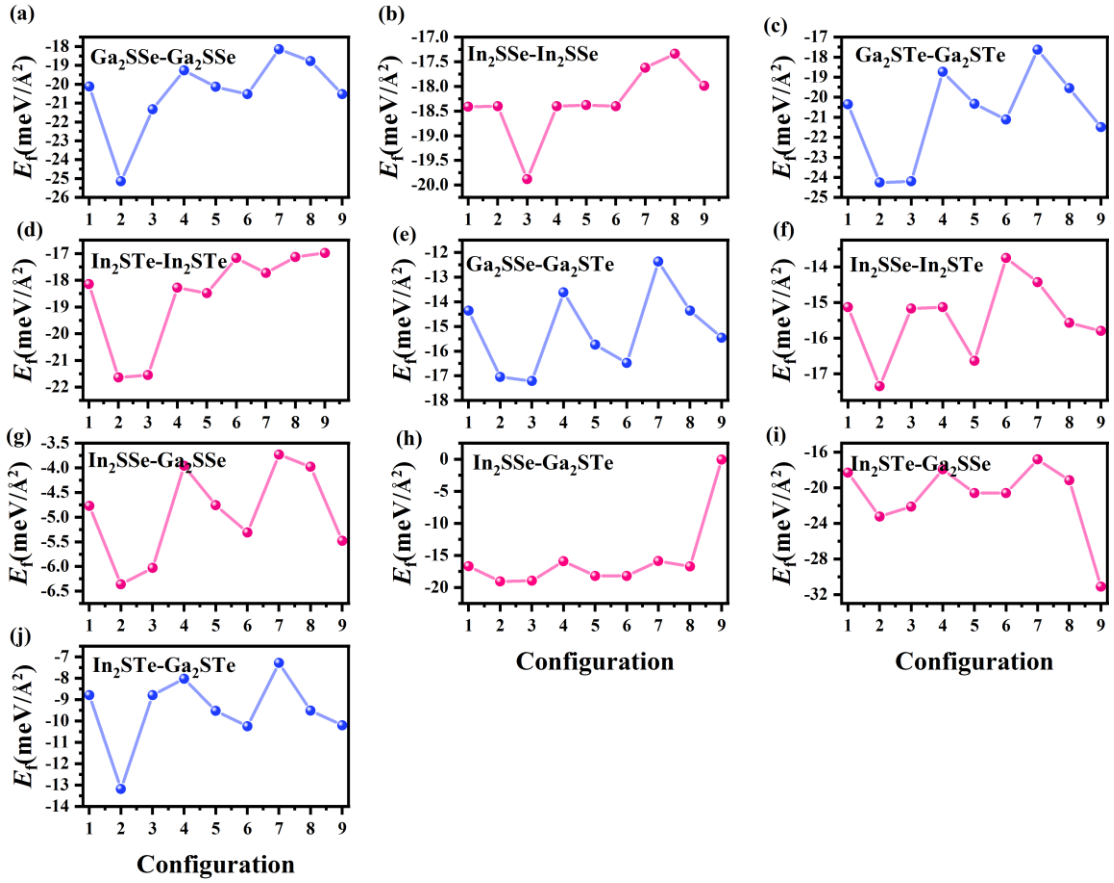

Fig. S4. The formation energies of the heterostructures with different stacking patterns. (a)Ga_2SSe-In_2SSe, (b) In_2SSe-In_2SSe, (c)Ga_2STe-Ga_2STe, (d) In_2STe-In_2STe, (e) Ga_2SSe-Ga_2STe, (f) In_2SSe-In_2STe, (g) In_2SSe-Ga_2SSe, (h)In_2SSe-Ga_2STe, (i) In_2STe-Ga_2SSe, (j) Ga_2STe - In_2STe.

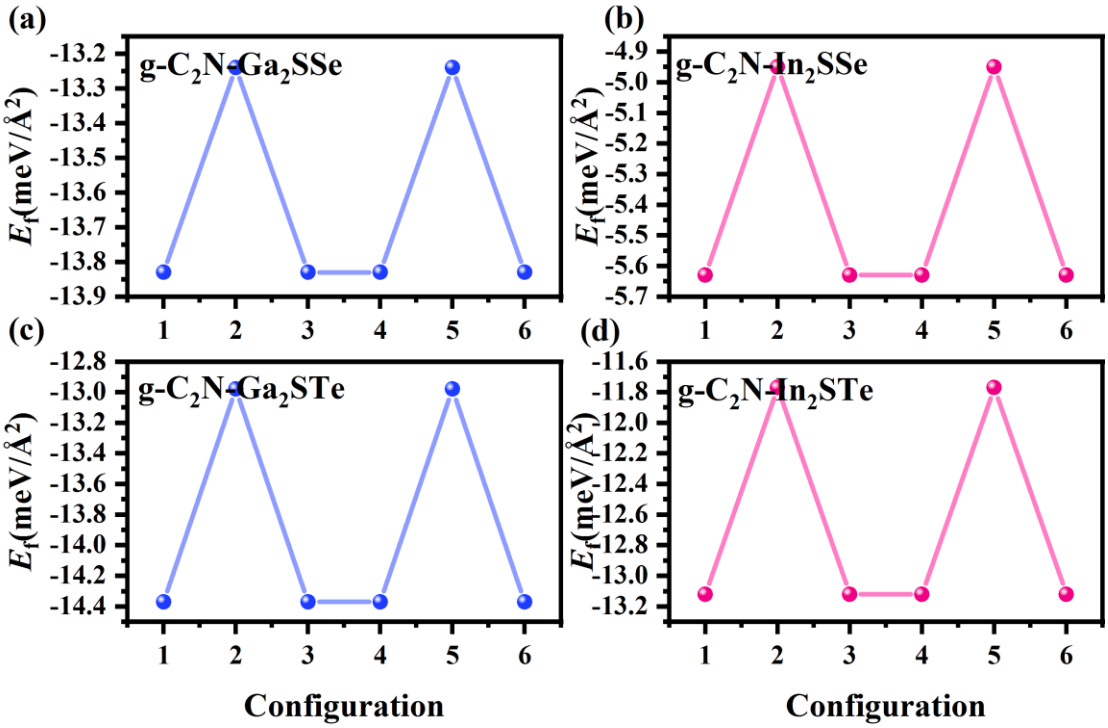

Fig. S5. The formation energies of the heterostructures with different stacking patterns. (a)g-C_2N-Ga_2SSe, (b) g-C_2N-In_2SSe, (c) g-C_2N-Ga_2STe, (d) g-C_2N-In_2STe.

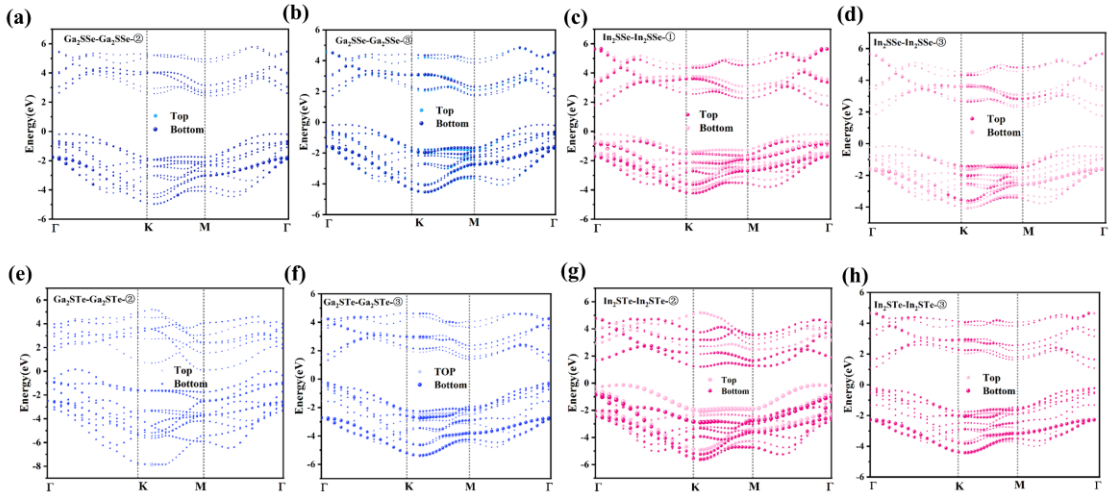

Fig. S6. The band structures of the heterostructure. (a) Ga_2SSe-Ga_2SSe-②, (b) Ga_2SSe-Ga_2SSe-③, (c) In_2SSe-In_2SSe-①, (d) In_2SSe-In_2SSe-③, (e) Ga_2STe-Ga_2STe-②, (f) Ga_2STe-Ga_2STe-③, (g) In_2STe-In_2STe-②, and (h) In_2STe-In_2STe-③.

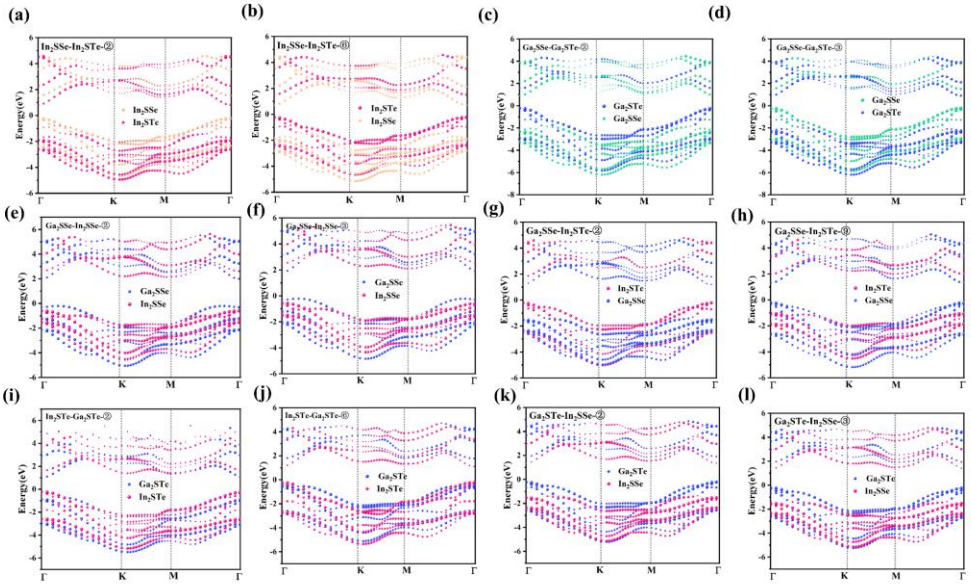

Fig. S7. The band structures of the heterostructures. (a) In_2SSe-In_2STe-②, (b) In_2SSe-In_2STe-⑤, (c) Ga_2SSe-Ga_2STe-②, (d) Ga_2SSe-Ga_2STe-③, (e) Ga_2SSe-In_2SSe-②, (f) Ga_2SSe-In_2SSe -③, (g) Ga_2SSe-In_2STe-②, (h) Ga_2SSe-In_2STe -⑨, (i) Ga_2STe -In_2STe-②, (j) Ga_2STe -In_2STe -⑥, (k) Ga_2STe-In_2SSe-②, and(l) Ga_2STe-In_2SSe-③.

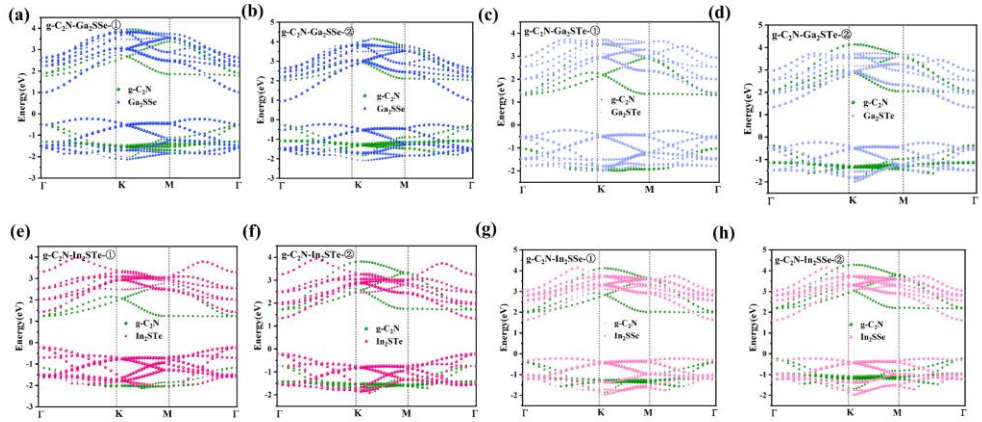

Fig. S8. The band structures of the heterostructures. (a) g-C_2N-Ga_2SSe-①, (b) g-C_2N-Ga_2SSe-②, (c) g-C_2N-Ga_2STe-①, (d) g-C_2N-Ga_2STe-②, (e) g-C_2N-In_2STe -①, (f) g-C_2N-In_2STe -②, (g)g-C_2N-In_2SSe,and (h) g-C_2N-In_2SSe.

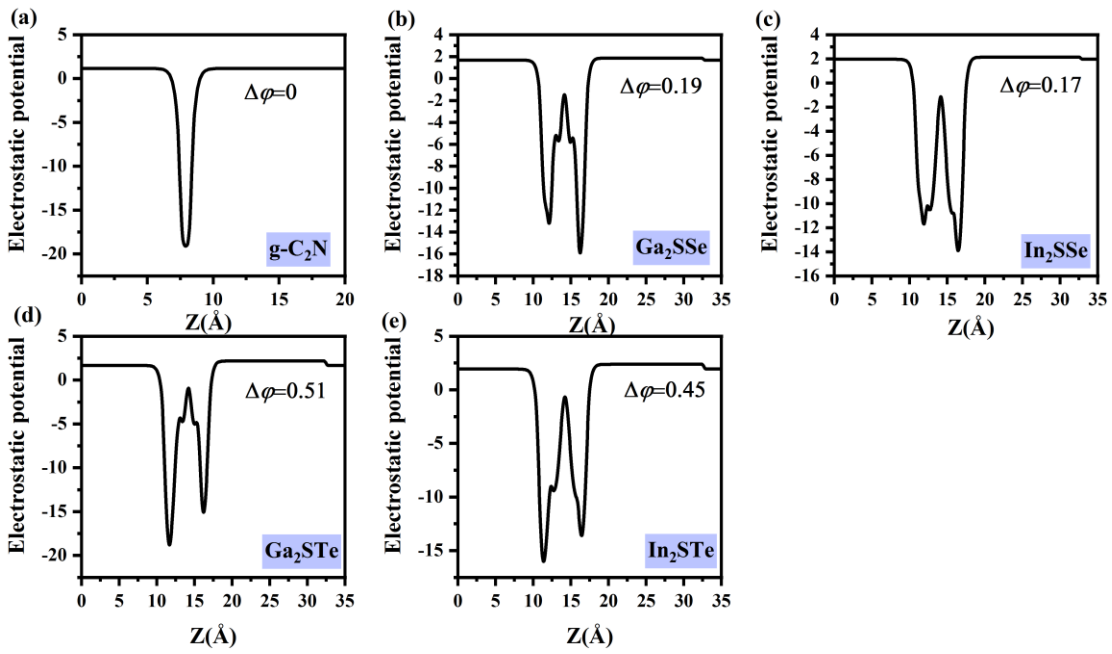

Fig. S9. The electrostatic potentials of the monolayers. (a) g-C_2N, (b) Ga_2SSe, (c) In_2SSe, (d) Ga_2STe, (e) In_2STe.

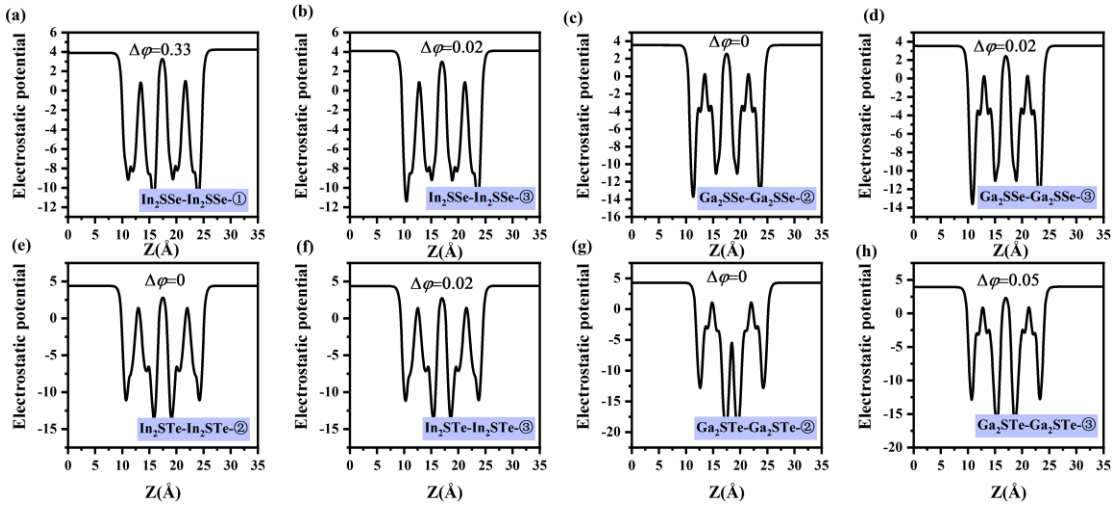

Fig. S10. The electrostatic potentials of the heterostructures. (a) In_2SSe-In_2SSe-①, (b) In_2SSe-In_2SSe-③, (c) Ga_2SSe-Ga_2SSe-②, (d) Ga_2SSe-Ga_2SSe-③, (e) In_2STe-In_2STe-②, (f) In_2STe-In_2STe-③, (g) Ga_2STe-Ga_2STe-②, and (h) Ga_2STe-Ga_2STe-③.

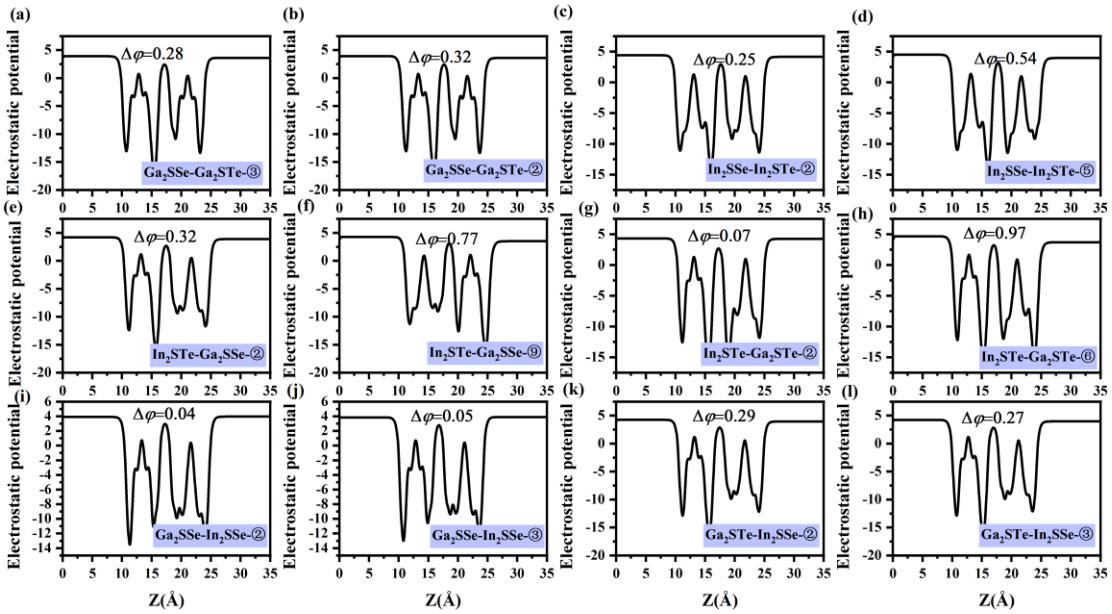

Fig. S11. The electrostatic potentials of the heterostructures. (a) Ga_2SSe-Ga_2STe-③, (b) Ga_2SSe-Ga_2STe-②, (c) In_2SSe-In_2STe-②, (d) In_2SSe-In_2STe-⑤, (e) Ga_2SSe-In_2STe-②, (f) Ga_2SSe-In_2STe -⑨, (g) Ga_2STe-In_2STe -②, (h) Ga_2STe-In_2STe -⑥, (i) Ga_2SSe-In_2SSe-②, (j) Ga_2SSe-In_2SSe -③, (k) Ga_2STe-In_2SSe-②, and(l) Ga_2STe-In_2SSe-③.

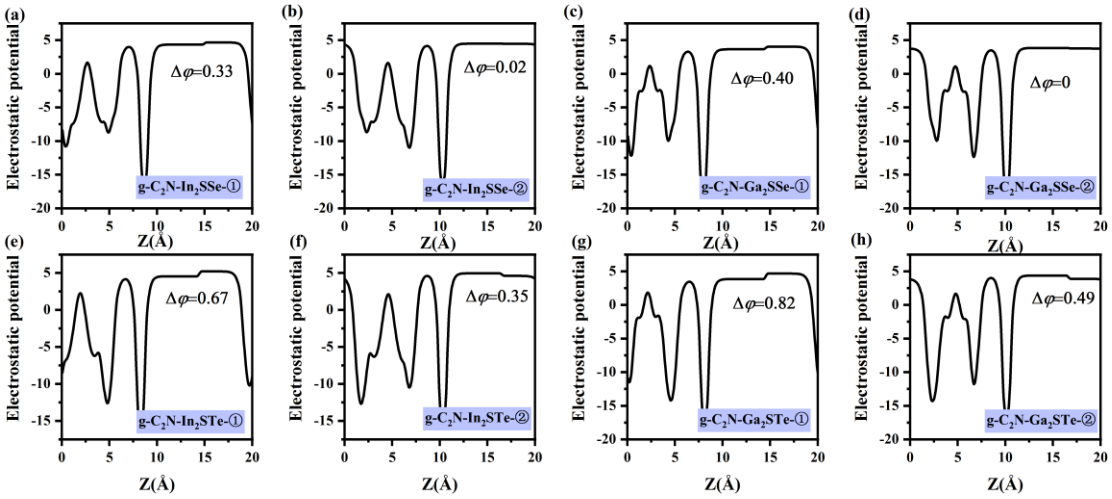

Fig. S12. The electrostatic potentials of the heterostructures. (a) g-C_2N-In_2SSe-①, (b) g-C_2N-In_2SSe-②, (c) g-C_2N-Ga_2SSe-①, (d) g-C_2N-Ga_2SSe-②, (e) g-C_2N-In_2STe -①, (f) g-C_2N-In_2STe -②, (g)g-C_2N-Ga_2STe, and (h) g-C_2N-Ga_2STe.

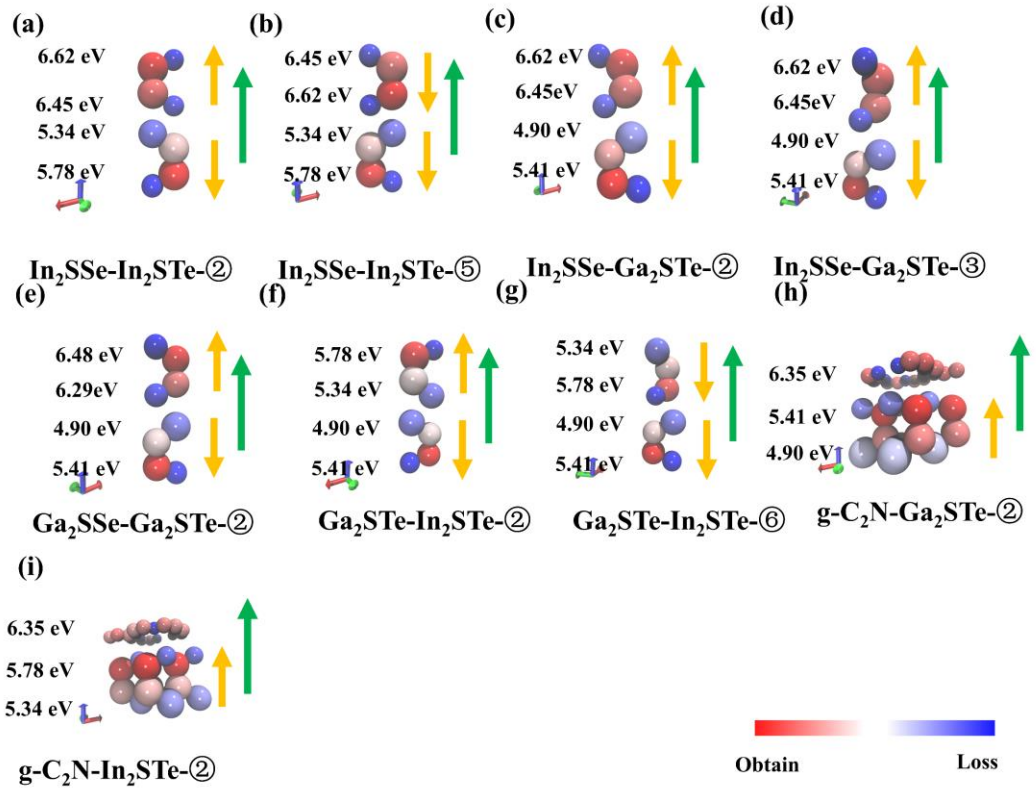

Fig. S13. The obtain or loss of charge in the atoms of every heterostructures with high PCE efficiency (>10%) calculated by Bader charge analysis and work function. The values on the right of every heterostructure is the work function. The atoms with red represent obtain electrons and the atoms with blue represent loss electrons. The yellow arrow represents the direction of intrinsic electronic filed and the green arrow represents the direction of E_{in}.

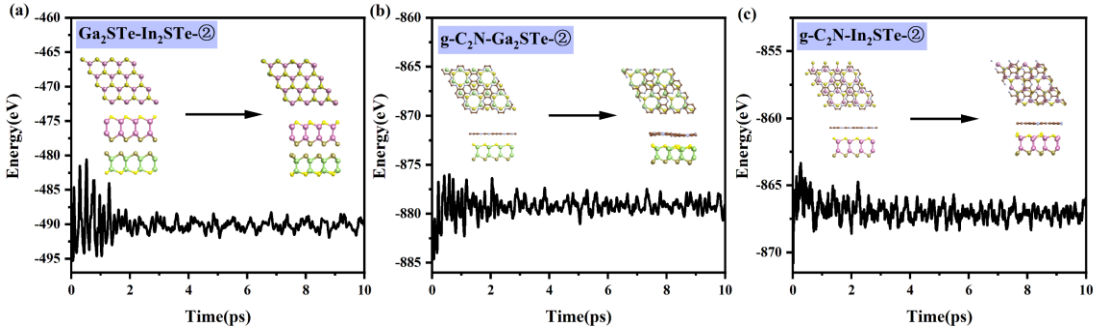

Fig. S14. The AIMD simulation results in a temperature of 300 K for the considered structures. (a)Ga_2STe-In_2STe-②, (b) g-C_2N-Ga_2STe-②, (c)g-C_2N-In_2STe-②

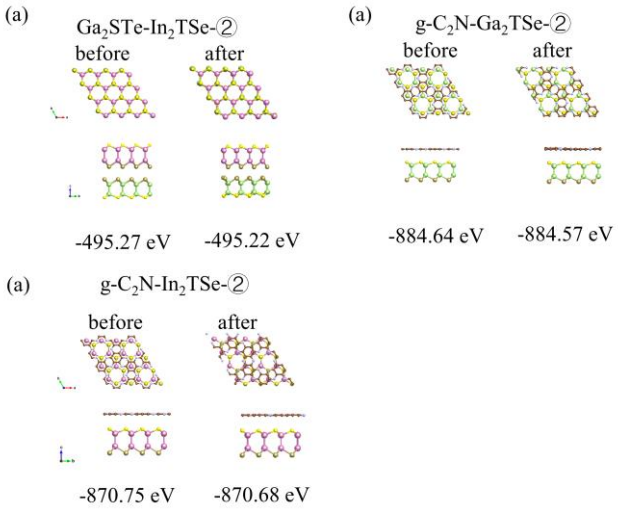

Fig. S15. The geometric structures and the energies of the heterostructures(the initial structures and final structures of the AIMD simulation) optimized at 0 K. (a)Ga_2STe-In_2STe-②, (b) g-C_2N-Ga_2STe-②, (c)g-C_2N-In_2STe-②.

Table S1 The lattice constants (a) and bandgaps (E_g) of the monolayers we considered.

Monolayer	a(this work) (Å)	a(other work) (Å)	E_g(this work) (E_g)	E_g(other work) (E_g)
g-C_2N	8.23	8.33[1]	2.54	2.49[2]
In_2SSe	3.92	3.86[3]	2.67	2.69[3]
In_2STe	4.06	4.02[3]	1.65	1.41[3]
Ga_2SSe	3.64	3.66[3]	3.17	3.29[3]
Ga_2STe	3.80	3.83[3]	1.75	1.59[3]

Table S2. The lattice constants (a), interlayer distances (d), and formation energies (E_f) of different configurations of different heterostructures.

Heterostructure	Configuration	a (Å)	d (Å)	E_f (eV)
	①	3.68	3.72	-20.12
	②	**3.68**	**3.80**	**-25.15**
	③	**3.68**	**3.77**	**-21.33**
	④	3.68	3.69	-19.27
Ga_2SSe-Ga_2SSe	⑤	3.68	3.72	-20.14
	⑥	3.68	3.69	-20.53
	⑦	3.68	3.66	-18.14
	⑧	3.68	3.65	-18.77
	⑨	3.68	3.65	-20.53
	①	**3.96**	**3.74**	**-18.41**
	②	3.96	3.80	-18.40
	③	**3.96**	**3.72**	**-19.88**
	④	3.97	3.68	-18.40
In_2SSe-In_2SSe	⑤	3.97	3.74	-18.38
	⑥	3.97	3.72	-
	⑦	3.97	3.62	-17.62
	⑧	3.95	3.61	-17.34
	⑨	3.97	3.68	-17.99
Ga_2STe-Ga_2STe	①	3.84	3.87	-20.36

	②	**3.84**	**3.96**	**-24.26**
	③	**3.85**	**3.95**	**-24.20**
	④	3.85	3.73	-18.73
	⑤	3.84	3.87	-20.33
	⑥	3.84	3.82	-21.11
	⑦	3.85	3.63	-17.63
	⑧	3.84	3.77	-19.55
	⑨	3.85	3.77	-21.50
	①	4.11	3.84	-18.15
	②	**4.10**	**3.95**	**-21.64**
	③	**4.11**	**3.92**	**-21.55**
	④	4.13	3.61	-18.28
In_2STe-In_2STe	⑤	4.11	3.84	-18.48
	⑥	4.09	3.71	-17.17
	⑦	4.12	3.60	-17.73
	⑧	4.10	3.71	-17.13
	⑨	4.10	3.63	-16.98
	①	3.76	3.75	-14.36
	②	**3.76**	**3.88**	**-17.05**
Ga_2SSe-Ga_2STe	**③**	**3.76**	**3.88**	**-17.21**
	④	3.76	3.69	-13.62
	⑤	3.76	3.87	-15.74

	⑥	3.76	3.77	-16.48
	⑦	3.77	3.61	-12.37
	⑧	3.76	3.77	-14.36
	⑨	3.77	3.64	-15.46
	①	4.04	3.73	-15.13
	②	**4.03**	**3.86**	**-17.35**
	③	4.03	3.75	-15.17
	④	4.04	3.67	-15.13
In_2SSe-In_2STe	**⑤**	**4.03**	**3.84**	**-16.64**
	⑥	4.03	3.70	-13.75
	⑦	4.04	3.67	-14.43
	⑧	4.03	3.70	-15.57
	⑨	4.04	3.68	-15.80
	①	3.82	3.75	-4.77
	②	**3.81**	**3.77**	**-6.36**
	③	**3.82**	**3.75**	**-6.03**
	④	3.82	3.68	-3.96
In_2SSe-Ga_2SSe	⑤	3.82	3.71	-4.76
	⑥	3.82	3.76	-5.31
	⑦	3.82	3.61	-3.73
	⑧	3.81	3.61	-3.98
	⑨	3.82	3.66	-5.48

	①	3.90	3.73	-16.69
	②	**3.89**	**3.86**	**-19.07**
	③	**3.90**	**3.84**	**-18.96**
	④	3.91	3.68	-15.91
In_2SSe-Ga_2STe	⑤	3.90	3.84	-18.20
	⑥	3.90	3.78	-18.21
	⑦	3.91	3.62	-15.89
	⑧	3.90	3.73	-16.73
	⑨	3.89	3.64	-0.06
	①	3.89	3.73	-18.31
	②	**3.73**	**3.87**	**-23.24**
	③	3.89	3.87	-22.12
	④	3.89	3.68	-17.93
In_2STe-Ga_2SSe	⑤	3.89	3.85	-20.60
	⑥	3.89	3.86	-20.60
	⑦	3.89	3.69	-16.83
	⑧	3.87	3.74	-19.17
	⑨	**3.90**	**3.66**	**-31.10**
	①	3.97	3.85	-8.79
	②	**3.97**	**3.93**	**-13.18**
Ga_2STe- In_2STe	③	3.97	3.97	-8.79
	④	3.98	3.66	-8.02

	⑤	3.97	3.86	-9.52
	⑥	**3.97**	**3.77**	**-10.25**
	⑦	3.98	3.63	-7.28
	⑧	3.97	3.81	-9.51
	⑨	3.97	3.83	-10.20
	①	**8.08**	**3.50**	**-13.83**
	②	**8.08**	**3.46**	**-13.24**
	③	8.08	3.50	-13.83
g-C_2N-Ga_2SSe	④	8.08	3.50	-13.83
	⑤	8.08	3.46	-13.24
	⑥	8.08	3.50	-13.83
	①	**8.22**	**3.47**	**-5.63**
	②	**8.22**	**3.44**	**-4.95**
	③	8.22	3.47	-5.63
g-C_2N-In_2SSe	④	8.22	3.47	-5.63
	⑤	8.22	3.44	-4.95
	⑥	8.22	3.47	-5.63
	①	**8.16**	**3.69**	**-14.37**
	②	**8.16**	**3.52**	**-12.98**
g-C_2N-Ga_2STe	③	8.16	3.69	-14.37
	④	8.16	3.69	-14.37
	⑤	8.16	3.52	-12.98

	⑥	8.16	3.69	-14.37
	①	**8.28**	**3.69**	**-13.12**
	②	**8.28**	**3.52**	**-11.77**
g-C_2N-In_2STe	③	8.28	3.69	-13.12
	④	8.28	3.69	-13.12
	⑤	8.28	3.52	-11.77
	⑥	8.28	3.69	-13.12

Table S3. The band alignment types, bandgaps (E_g), conduction band offsets (ΔE_c), open circuit voltage (V_{oc}) and η_{PCE} of different configurations of different heterostructures.

Heterostructure	configuration	Band alignment	E_g (eV)	ΔE_c (eV)	V_{oc} (eV)	η_{PCE} (%)
In_2SSe-In_2SSe	①	II	2.63	0.32	2.31	6.72
	③	--	--		--	--
Ga_2SSe-	②	--	--		--	--
Ga_2SSe	③	--	--		--	--
In_2STe-In_2STe	②	--	--		--	--
	③	--	--	--	--	--
Ga_2STe-	②	--	--	--	--	--
Ga_2STe	③	--	--	--	--	--
Ga_2SSe-	**②**	**II**	**1.82**	**0.37**	**1.46**	**14.63**
Ga_2STe	③	II	2.17	0.77	1.39	8.20
In_2SSe-In_2STe	**②**	**II**	**1.74**	**0.46**	**1.28**	**13.81**

	⑤	**II**	**1.73**	**0.28**	**1.46**	**16.57**
In_2SSe-Ga_2SSe	②	I	3.69	1.06	2.55	0.37
	③	I	3.55	1.14	2.07	0.63
In_2SSe-Ga_2STe	**②**	**II**	**2.08**	**0.20**	**1.88**	**13.47**
	③	**II**	**2.10**	**0.27**	**1.82**	**12.73**
In_2STe-Ga_2SSe	②	II	2.73	0.99	1.74	3.89
	⑨	I	3.03	0.09	1.53	4.02
Ga_2STe-In_2STe	**②**	**II**	**1.63**	**0.47**	**1.16**	**14.06**
	⑥	I	2.24	0.32	1.33	10.73
g-C_2N-In_2SSe	**①**	**I**	**2.38**	**0.01**	**1.87**	**10.83**
	②	II	2.38	0.54	1.84	8.01
g-C_2N-Ga_2SSe	①	I	3.10	0.37	1.21	3.23
	②	I	2.27	0.98	1.18	6.23
g-C_2N-In_2STe	①	II	1.65	0.88	0.78	7.60
	②	**I**	**2.42**	**0.07**	**1.45**	**10.07**
g-C_2N-Ga_2STe	①	II	2.33	0.41	2.35	9.30
	②	**I**	**2.30**	**0.12**	**1.56**	**11.30**

2. Calculational details for the optical properties and the solar-to-hydrogen conversion efficiency (η'_{STH})

The equation of optical absorption coefficient $\alpha(\omega)$ is [4,5]

$$\alpha(\omega) = \sqrt{2}\sqrt{\sqrt{\varepsilon_r^2(\omega) + \varepsilon_i^2}(\omega) - \varepsilon_r(\omega)} \quad (1)$$

Where $\varepsilon_i(\omega)$ is the imaginary part of the complex dielectric function $\varepsilon(\omega) =$

$\varepsilon_r(\omega) + i\varepsilon_i(w)$, can be calculated by the following equation [6]:

$$\varepsilon_i(\omega) = \frac{4\pi^2}{m^2\omega^2}\Sigma_{c,v}\int_{Bz}\frac{2}{(2\pi)^3}\left|M_{c,v}(k)\right|^2\delta(\varepsilon_{ck} - \varepsilon_{vk} - h_\omega)d^3k \quad (2)$$

Where $\left|M_{c,v}(k)\right|^2$ represent the momentum matrix element, *c*, and *v* represent the conduction and valence band states, respectively. $\varepsilon_i(\omega)$ can be calculated by VASP. The real part $\varepsilon_r(\omega)$ can be calculated from the imaginary part $\varepsilon_i(\omega)$ of the complex dielectric function by using the Kramer-Kroning relationship [7].

3. Calculational detail of the NAMD simulation

The nonadiabatic molecular dynamics (NAMD) simulation for the carrier transfer and the electron-hole recombination were carried out by Hefei-NAMD code [8]. The average nonadiabatic coupling (NAC) matrix elements are defined as

$$\mathbf{d}_{ij} = \left\langle \varphi_i \left| \frac{\partial}{\partial t} \right| \varphi_j \right\rangle = \frac{\left\langle \varphi_i \left| \nabla_R \widehat{H} \right| \varphi_j \right\rangle}{\varepsilon_j - \varepsilon_i}\dot{\mathbf{R}} \quad (3)$$

Where $\mathbf{d}_{ij}$ is the NAC between states *i* and *j*, $\widehat{H}$ is the electronic Hamiltonian, φ_{ij}, ε_{ij}, are the wave functions and energies of electronic states i/j, and $\dot{\mathbf{R}}$ is the velocity of the nuclear.

The decoherence time was computed as the pure-dephasing time in the optical response formalism [9]. The fluctuations are characterized by the energy gap autocorrelation function (ACF) which defined by [10]

$$C_{(t)} = \frac{\langle \delta U(t)\delta U(t_0)\rangle_T}{\left\langle \left(\delta U(t_0)\right)^2 \right\rangle_T} = \frac{C_{un}(t)}{\langle \Delta E^2(0)\rangle_T} \quad (4)$$

δU is the deviation of the energy gap from the average value, $C_{un}(t)$ is the unnormalized ACF, $C_{(t)}$ is the normalized ACF [11].

$$\delta U(t) = \Delta E_{ij}(\mathbf{R}(t)) - \langle \Delta E_{ij}(\mathbf{R}(t)) \rangle_T \quad (5)$$

The ΔE_{ij} is the energy difference between the i and j states, and **R**(t) is determined through the quantum force.

$$D(t) = exp\left[-\frac{\langle (\delta U)^2 \rangle_T}{\hbar^2} \int_0^t d\tau_2 \int_0^{\tau_2} d\tau_1 \, C(\tau_1) \right] \quad (6)$$

The pure-dephasing time got by fitting Eq. 13 with the Gaussian function, exp(-0.5(t/τ)).

The spectral density was calculated by applying the Fourier transform of an ACF function [12],

$$I(\omega) = \left| \frac{1}{\sqrt{2\pi}} \int_{-\infty}^{+\infty} dt \, e^{-i\omega t} C(t) \right|^2 \quad (7)$$

66 cm^{-1} **110 cm^{-1}**

Fig. S16 The vibration modes of Ga_2STe - In_2STe -② calculated by VASP.

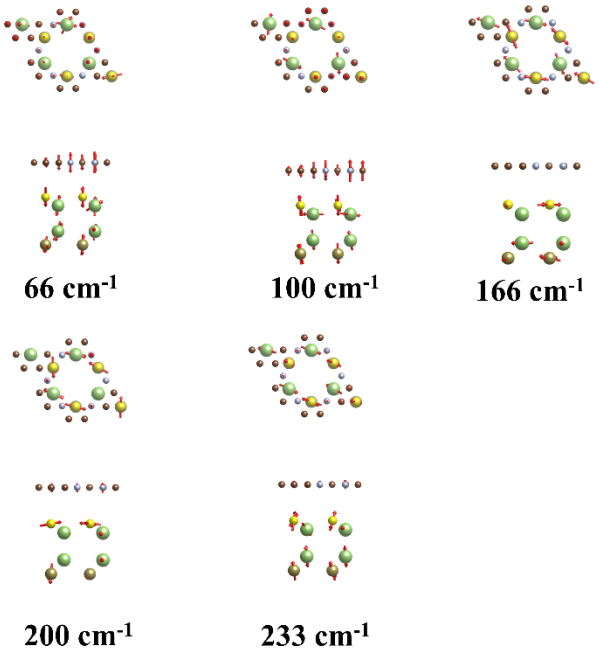

Fig. S17 The vibration modes of g-C_2N-Ga_2STe-② calculated by VASP.

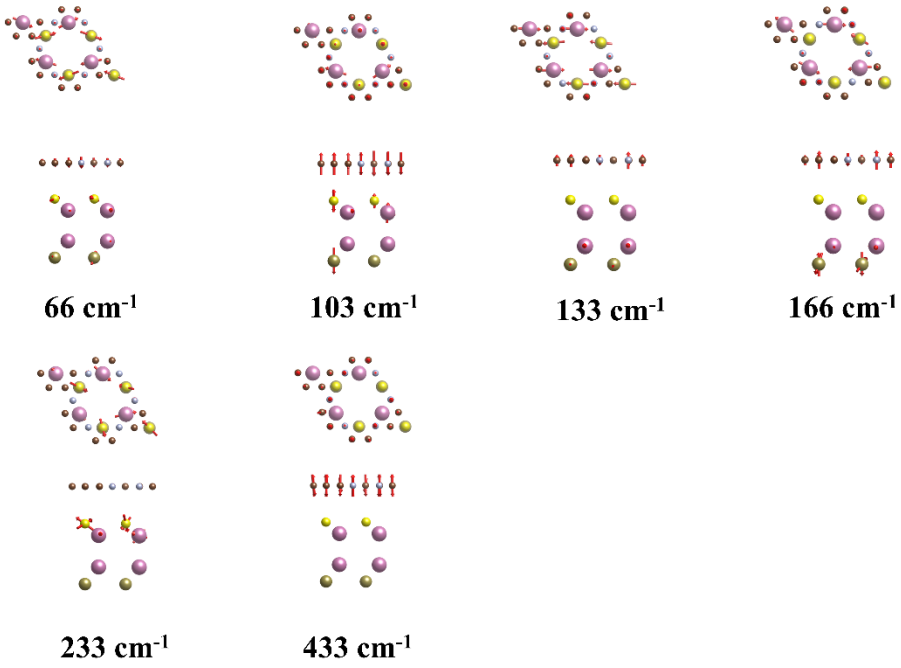

Fig. S18 The vibration modes of g-C_2N-In_2STe-② calculated by VASP.

4. Details and calculational results of the carrier mobility

We calculated the carrier mobility of the three monolayers using the deformation potential (DP) theory [12]. The equation is [13-14]

$$\mu = \frac{2e\hbar^3 C}{3k_B T|m^*|^2 E_d^2} \quad (8)$$

Where the carrier mobility μ depends on the elastic modulus C, effective mass m^*, and deformation potential constant E_{d}. e, $\hbar$, k_B, and T are the electron charge, the reduced Planck constant, the Boltzmann constant, T is the temperature was set as 300 K. C, m^*, E_{d}, defined as $C = \frac{1}{S_0}\frac{\partial^2 E}{\partial \varepsilon^2}$, $\frac{1}{m^*} = \frac{1}{\hbar}\frac{\partial^2 E(k)}{\partial k^2}$, $E_{\mathrm{d}} = \frac{\partial E_{edge}}{\partial \varepsilon}$, respectively. For the above equation C, m^*, E_d, where ε is the ratio of lattice parameter under the uniaxial

strain along x or y direction on the rectangle cell, E is the total energy of the monolayer under uniaxial strains, S_0 is the area of the monolayer, and $E(k)$ is the energy corresponding to k, k is the wave vector. E_{edge} is the energy of the band edge position calculated by HSE06. The detailed results are shown in Fig. S19–S23.

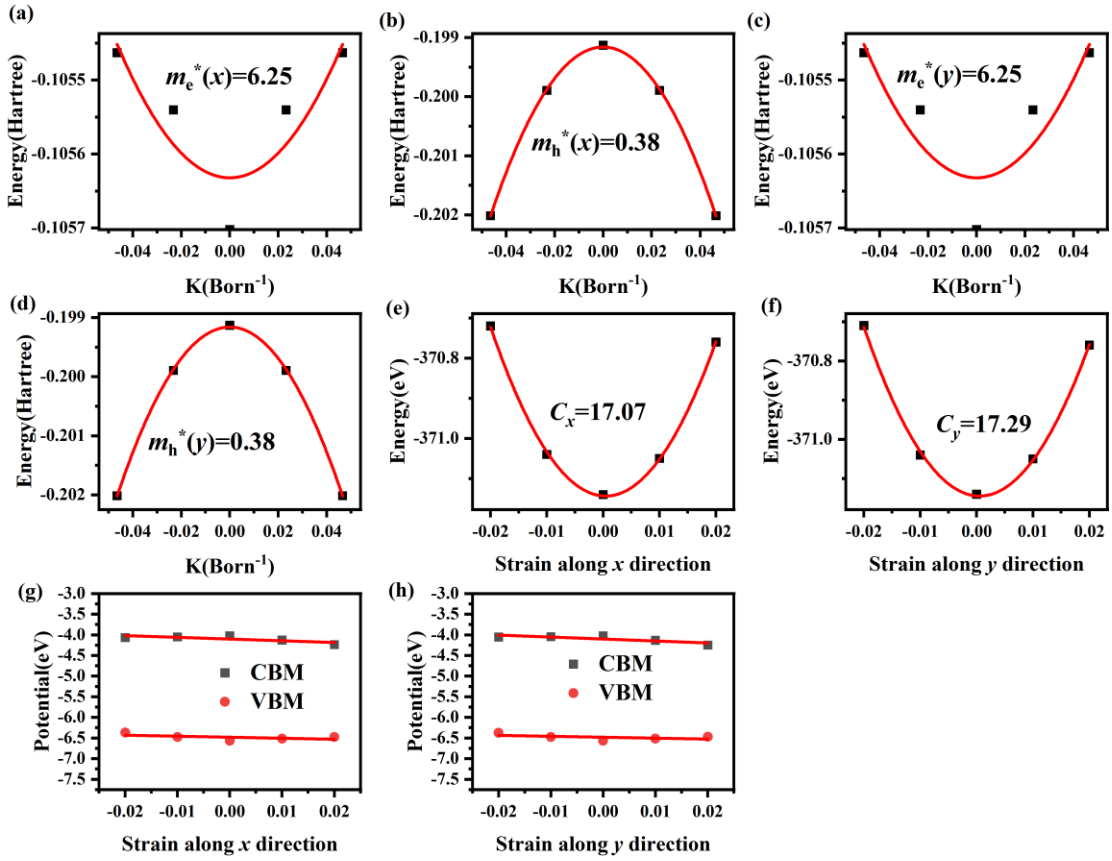

Fig. S19. The fitting curve of elastic constant (C), deformation potential constant (E_d), and effective mass (m*) of the g-C_2N monolayer. (a) and (b) are the m* fitting curves of the electrons and holes along the x directions, respectively. (c) and (d) are the m* fitting curves of the electrons and holes along the y directions, respectively. (e) and (f) are the fitting curves of C along the x and y directions, respectively. (g) and (h) are the fitting curves of E_d along the x and y directions, respectively.

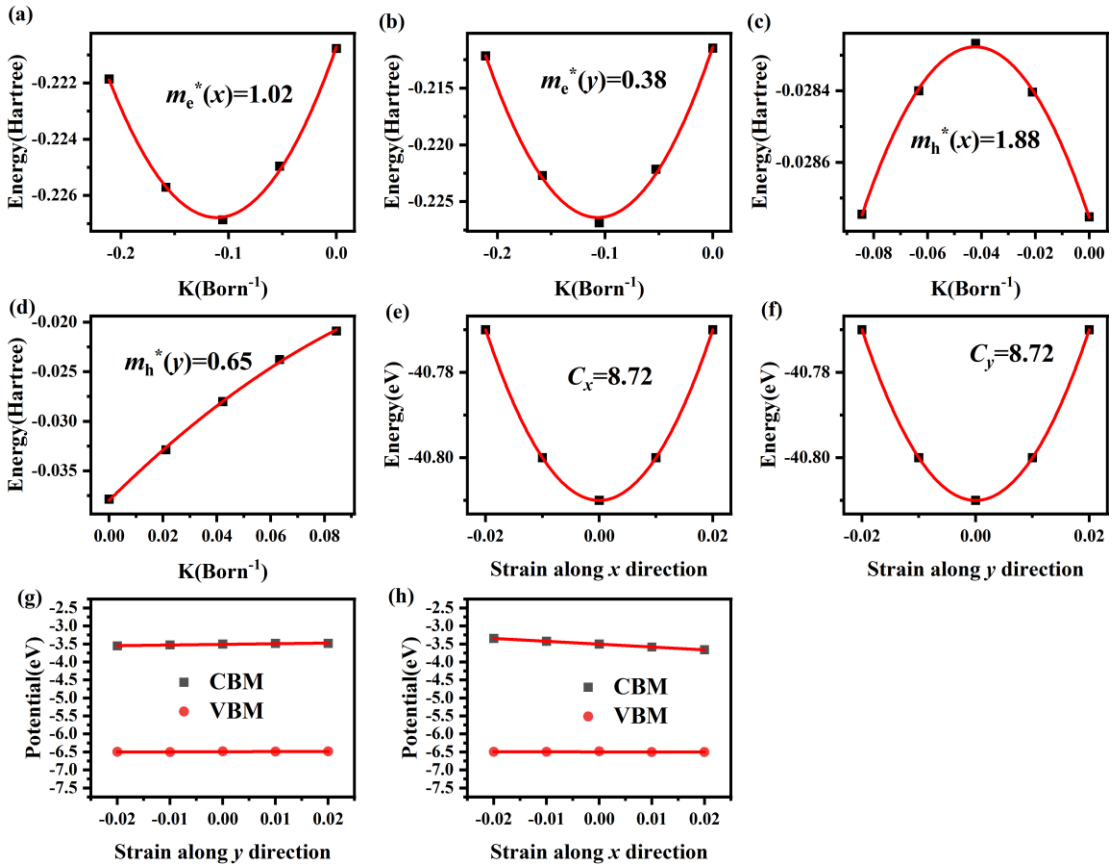

Fig. S20. The fitting curve of elastic constant (C), deformation potential constant (E_d), and effective mass (m*) of the Ga_2SSe monolayer. (a) and (b) are the m* fitting curves of the electrons and holes along the x directions, respectively. (c) and (d) are the m* fitting curves of the electrons and holes along the y directions, respectively. (e) and (f) are the fitting curves of C along the x and y directions, respectively. (g) and (h) are the fitting curves of E_d along the x and y directions, respectively.

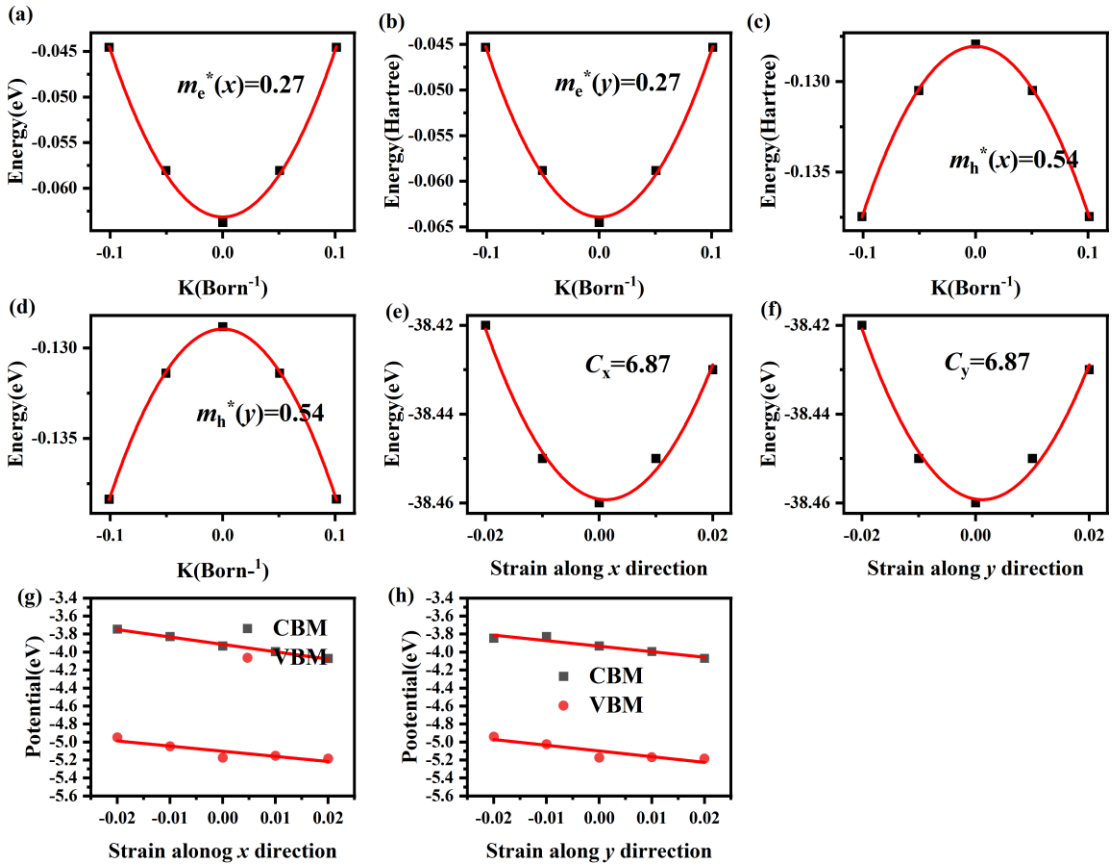

Fig. S21. The fitting curve of elastic constant (C), deformation potential constant (E_d), and effective mass (m*) of the Ga_2STe monolayer. (a) and (b) are the m* fitting curves of the electrons and holes along the x directions, respectively. (c) and (d) are the m* fitting curves of the electrons and holes along the y directions, respectively. (e) and (f) are the fitting curves of C along the x and y directions, respectively. (g) and (h) are the fitting curves of E_d along the x and y directions, respectively.

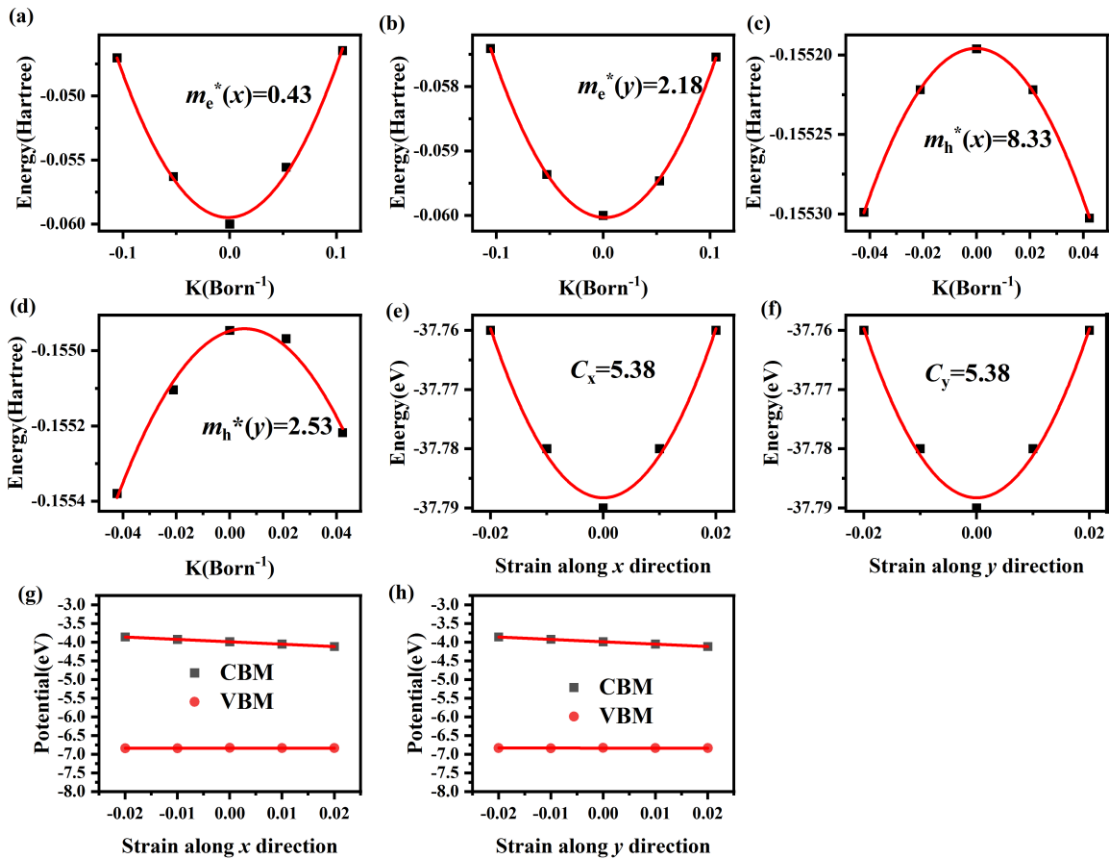

Fig. S22. The fitting curve of elastic constant (C), deformation potential constant (E_d), and effective mass (m^*) of the In_2SSe monolayer. (a) and (b) are the m^* fitting curves of the electrons and holes along the x directions, respectively. (c) and (d) are the m^* fitting curves of the electrons and holes along the y directions, respectively. (e) and (f) are the fitting curves of C along the x and y directions, respectively. (g) and (h) are the fitting curves of E_d along the x and y directions, respectively.

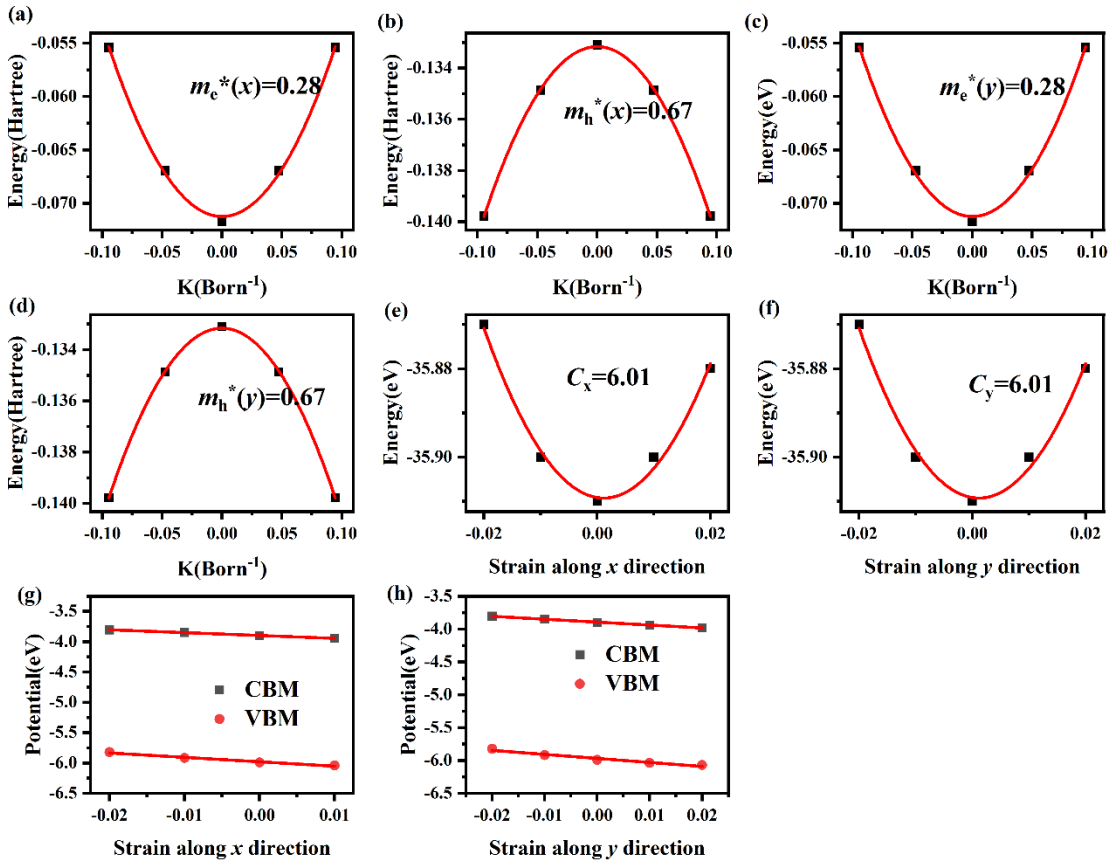

Fig. S23. The fitting curve of elastic constant (C), deformation potential constant (E_d), and effective mass (m^*) of the In_2STe monolayer. (a) and (b) are the m^* fitting curves of the electrons and holes along the x directions, respectively. (c) and (d) are the m^* fitting curves of the electrons and holes along the y directions, respectively. (e) and (f) are the fitting curves of C along the x and y directions, respectively. (g) and (h) are the fitting curves of E_d along the x and y directions, respectively.

Table S4. The elastic modulus (C), deformation potential constant (E_d), effective mass (m^*), and carrier mobility (μ) for the monolayers along with the x and y directions at 300 K.

Monolayer	Direction	Carrier	C (N/m)	E_d (eV)	m^* (m_0)	μ ($cm^2V^{-1}s^{-1}$)
g-C_2N	x	electron	281.66	4.18	6.25	5.68
		hole	281.66	2.46	0.38	4443.76
	y	electron	285.29	4.77	6.25	4.43
		hole	285.29	2.23	0.38	5477.37
Ga_2SSe	x	electron	8.72	7.94	1.02	346.83
		hole	8.72	0.18	1.88	198652.19
	y	electron	8.72	1.81	0.38	48087.22
		hole	8.72	0.44	0.65	278113.46
In_2SSe	x	electron	5.38	6.38	0.43	2159.02
		hole	5.38	0.10	8.33	23417.73
	y	electron	5.38	6.35	2.18	84.79
		hole	5.38	0.04	2.53	1586622.85
Ga_2STe	x	electron	6.87	8.21	0.27	3968.00
		hole	6.87	5.71	0.54	2050.81
	y	electron	6.87	6.13	0.27	7117.66
		hole	6.87	6.35	0.54	1658.25
In_2STe	x	electron	6.01	4.71	0.28	11210.57
		hole	6.01	4.44	0.67	1264.85

	y	electron	6.01	5.86	0.28	7242.26
		hole	6.01	5.97	0.67	1218.67

References

1. Z. Zheng, X. Wang, W. Mi. Electric field tunable electronic structure in two-dimensional van der Waals g-C_2N/XSe_2 (X= Mo, W) heterostructures. *Carbon*, 2017, **117**, 393-398.
2. D. Wang, D. X. Han, L. Liu, et al. Structure and electronic properties of C_2 N/graphene predicted by first-principles calculations. *RSC Adv*. 2016, **6(34)**, 8484-28488.
3. X. Liu, P. Cheng, X. Zhang, et al. Enhanced solar-to-hydrogen efficiency for photocatalytic water splitting based on a polarized heterostructure: the role of intrinsic dipoles in heterostructures. *J. Mater. Chem. A*, 2021, **9(25)**, 14515-14523.
4. S. Saha, T. P. Sinha, A. Mookerjee. Electronic structure, chemical bonding, and optical properties of paraelectric $BaTiO_3$. *Phys. Rev. B*. 2000, **62**, 8828-8834.
5. P. Li, C. W. Zhang, J. Lian, et. al. First-principal study of optical properties of Cu-doped CdS. *Opt Commun*, 2013, **295**, 45-52.
6. Y. Li, Z. Chen. Tuning electronic properties of germanane layers by external electric field and biaxial tensile strain: a computational study. *J. Phys. Chem. C*. 2014, **118**, 1148.
7. Q. Zheng, W. Chu, C. Zhao, et al. Ab initio nonadiabatic molecular dynamics investigations on the excited carriers in condensed matter systems. *Wiley*

Interdiscip. Rev.: Comput. Mol. Sci. 2019, **9**, e1411.

8. R. Long, O. V. Prezhdo, Quantum coherence facilitates efficient charge separation at a MoS_2/$MoSe_2$ van der Waals junction. *Nano Lett*. 2016, **16**, 1996−2003.
9. H. M. Jaeger, S. Fischer, O. V. Prezhdo. Decoherence-induced surface hopping. *J. Chem. Phys*. 2012, **137**, 22A545.
10. J. Bardeen, W. Shockley. Deformation potentials and mobilities in nonpolar crystals. *Phys. Rev*. 1950, **80**, 72.
11. S. Bruzzone, G. Fiori. *Ab initio* simulations of deformation potentials and electron mobility in chemically modified graphene and two-dimensional hexagonal boron-nitride. *Appl. Phys. Lett*. 2011, **99**, 222108.
12. J. Chen, J. Xi, D. Wang, et. al. Carrier mobility in graphene should be even larger than that in graphene: a theoretical prediction. *J. Phys. Chem. Lett*. 2013, **4** , 1443-1448.
13. J. Dai, X. C. Zeng. Titanium trisulfide monolayer: theoretical prediction of a new direct gap semiconductor with high and anisotropic carrier mobility. *Angew. Chem*. 2015, **54**, 7572–7576.